Medical image reconstruction using an exact formula for solid angle of view

S. ZIMERAS
University of the Aegean
Department of Statistics and Actuarial-Financial Mathematics
G.R.832 00, Karlovassi, Samos,
GREECE

*Abstract***:** Modeling of the tomographic weights usually incorporates angle of view, decay and attenuation. A usual assumption is that the gamma camera is a long way from the object, this leads to the approximation that the angle of view subtending the front of the collimator tube is the same as that subtending the back [6]. If, however, the distance between camera and subject is small then this approximation may not be good enough and artifacts may be produced.
In this paper, the derivations of the angle of view and the solid angle of view are analyzed considering distances when the camera is close to the body. The solid angle is explained by an appropriate formula which is defined as the exact solid angle of view. The effect of the solid angle of view for different distances is examined. A comparison between exact solid angle and the approximate solid angle formula of Weir is presented. Finally the effects of the two formulae on reconstruction are studied using simulated data from circular gamma camera rotation systems.

Keywords: Tomographic weight, solid angle, medical imaging, contour orbit, emission tomography.

1 Introduction

Medical techniques play an important role in clinical diagnosis, allowing the study and treatment of diseases. In addition, over the last decade improvements in medical imaging devices have helped in the investigation of clinical problems, explanation of the functional process of organs and study of the human body.
Reliable reconstruction depends on detailed knowledge of the weights. Accurate modeling of the weights is important since in practice they are unknown. Modeling of the tomographic weights usually incorporates geometric angle of view, radioactive particle decay, scatter and attenuation [1, 2]. Assuming "good geometry" conditions [3, 4] scatter is negligible and attenuation uniform to the entire image plane. In all cameras the images, produced by an object of given shape, is dependent on the position of the object. This dependence is due to both the characteristics of the collimator and the position of the camera detector. It is common to assume that the gamma camera is a long way from the subject; this leads to the approximation that the angle subtending the front of the collimator tube is the same as that subtending the back. If however, the distance between camera and subject is small, then this approximation may not be good enough and artifacts may be produced [1].
In this work a derivation of the exact solid angle of view is studied for distances when the camera is close to the body. The effects of the solid angle of view for different distances are examined and a comparison between exact and approximate solid angle formula of view is presented. Finally an analysis of various distances using different camera measurements is presented for both formulae.

2 Physics of gamma camera

Gamma camera imaging is a modern medical diagnostic technique, based to study function rather than form. The patient is injected with or inhales an appropriate drug, which became concentrated in the organ of interest. Photons emission occurs in the organ at a rate ranging spatially according to the concentration and measurements of this concentration can be made by counting emitted photons in the gamma camera. The physical and operational details of the gamma camera are

described by [5]. The gamma camera rotated about an axis through the patient to collect a sequence of projections from the body at numerous equally spaced angles. The session begins with the gamma camera directly above and facing the patient. In this potion, the camera detects and records photons leaving the patient's body in a certain time period after 20 seconds. The camera then rotates about an axis parallel to the table, stops after 64 degrees and collects counts at the new angle. This process is repeated until the gamma camera return to its original position directly above the patient. The majority of emissions are never recorded by the system since their path is not towards the camera. The camera has a lead parallel-hole collimator which further limits the number of recorded emissions by only emitted photons whose path is nearly exactly perpendicular to the surface of the camera. Figure 1 demonstrates the basic component of a gamma camera and the various paths that an emitted photon can take: (1) photon emitted away from the camera, (2) photon emitted and scattered away from the camera, (3) photon absorbed inside the subject, (4) photon emitted away from the camera but scattered through collimator, (5) photon emitted directly through the collimator, (6) photon directed towards camera, but at an angle preventing it from passing through collimator.

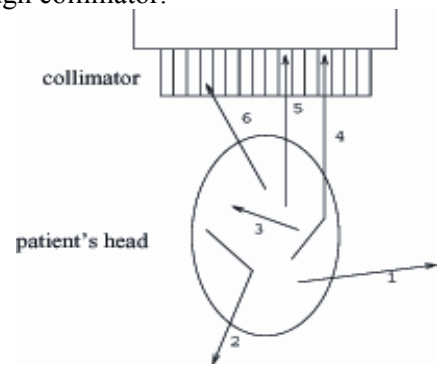

Figure 1. Detection of photons in the gamma camera: (1) photon emitted away from the camera, (2) photon emitted and scattered away from the camera, (3) photon absorbed inside the subject, (4) photon emitted away from the camera but scattered through collimator, (5) photon emitted directly through the collimator, (6) photon directed towards camera, but at an angle preventing it from passing through collimator.

The method of data collection means that the 3D object is divided up into multiple 2D projections and each projection is represented by a set of discrete 1D profile. Each point on the profile represents the linear sum, in the absence of attenuation, of the emissions along the line of view of the detectors through the collimator. A common way of displaying the data is by taking all 1D profile corresponding to a cross sectional slice through the object. This type of representation has been referred to as a sinogram, where the horizontal axis represents camera angles and the vertical the detectors along each 1D cross-sectional profile.

3 Derivation of solid angle of view

One of the important factors for the weight calculations is the solid angle of view, which is defined as the 3-dimensional angle of view. Assuming that the detectors are modeled as cylindrical tubes and the subject is divided into equal rectangular grid, then the solid angle of view depends on four factors (Figure 2): (1) distance t of pixel from tube axis; (2) distance s along tube axis between tube and perpendicular from pixel; (3) radius q of tube and (4) half-distance p of tube.

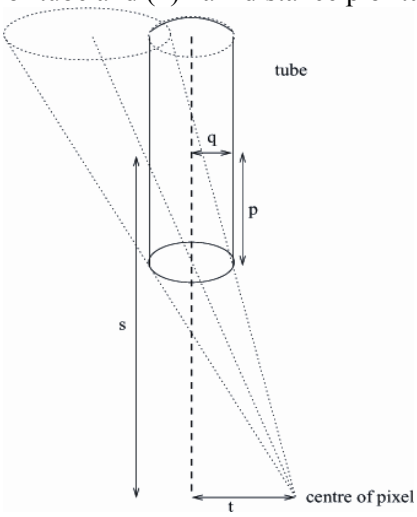

Figure 2. Geometry of solid angle of view: The solid angle is determined by the area of overlap between the back of the detector tube and the projection of the front of the tube.

The solid angle of view is measured by the area A of the back of the tube visible from the body pixel. Thus the solid angle from a pixel to a detector, θ(s,t) is given by: $\theta(s,t) = \tan^{-1}\left[\frac{A}{(s+p)^2}\right]$, where $0 \le \theta(s,t) \le \tan^{-1}\left[\pi\frac{q^2}{(s+p)^2}\right]$ and A denotes the intersection area between the front and the back disc of the tube cylinder when viewed from the pixel. When θ(s,t) is very small, the first order approximation gives: $\theta(s,t) \approx \left[\frac{A}{(s+p)^2}\right]$. Consider the

detector tube as represented by two discs, one corresponding to the back of the tube and the second the projection of the front of the tube onto the plane which passes through the back of the tube (Figure 2). The intersection of these discs defines the overlap area A. In [6] authors have investigated the case where the camera is far away from the body. For this case they calculate the solid angle based on the assumption that the two discs of the tube are equal. In this case the solid angle formula works successfully when the camera is a long way from the body. If the distance between camera and body is small the above assumption is not true. In this case the two discs are not equal.

4 Exact solid angle of view

For the derivation of exact solid angle three cases are considered (Figure 3): (1) if the ratio $q/p < t/s$ then the discs do not overlap and the solid angle is zero, (2) if the ratio $q/p \geq t/s$ and $t \leq q$ then the rear disc is inside the projection of the front and the solid angle is given by $\theta(s,t) = \tan^{-1}\left[\frac{A}{(s+p)^2}\right]$, (3) if the ratio $q/p > t/s$ and $t > q$, then the two discs intersect and the solid angle is given by the following calculation.

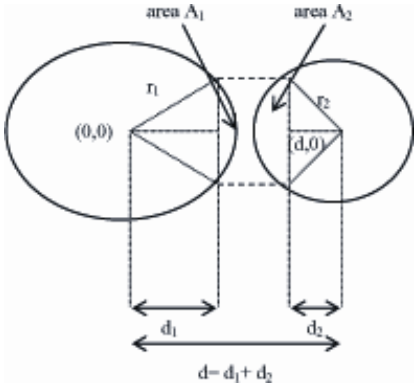

Figure 4. Geometry of the two non-equal discs. The overlap area is obtained from the two segments which are defined by the line passing through the points of intersection of the circles.

In the intersecting case, the two circles can be expressed by a system of equations, where the first disc is center at the (0,0) and the second at the (d,0) (Figure 4); r_2 is the radius of the tube, r_1 is the radius of the projection of the front of the tube and d is the distance between the centers of the discs. The distance d is given by the sum of distances d_1 and d_2 which denote the perpendicular distances from the center of the first and second discs of the chords. The solution of the system equation gives the intersection points between the two circles. By elementary trigonometry, it can be shown that the three unknown parameters (d, r_1, r_2) are given by: $d = \left[\frac{2p}{s-p}\right]t$, $r_1 = q$, $r_2 = \left[\frac{s+p}{s-p}\right]q$ [7]. The overlap area $A = A_1 + A_2$ for the two non-equal discs radius r_1, r_2 and centers d_1+d_2 is given by:

$A = \frac{1}{2}r_1^2\left\{f_1\left(d_1/r_1\right)\right\} + \frac{1}{2}r_2^2\left\{f_2\left(d_2/r_2\right)\right\}$, where

$f_i\left(d_i/r_i\right) = 2\left\{\cos^{-1}\left(d_i/r_i\right) - \left(d_i/r_i\right)\sqrt{1-\left(d_i/r_i\right)^2}\right\}$ i=1, 2,

$d_1 = \frac{d^2 + r_1^2 - r_2^2}{2d}$, and $d_2 = d - d_1$. Having found the overlap area, the formula for the solid angle is given by [7]:

$$\theta(s,t)^{exact} = \left[\frac{q^2}{(s+p)^2}\right] f_1\left\{\frac{t^2 p - sq^2}{tq(s-p)}\right\} + \left[\frac{q^2}{(s-p)^2}\right] f_2\left\{\frac{t^2 p - sq^2}{tq(s+p)}\right\}.$$

The resulting shape of the solid angle function appears to be a Gaussian curve. The normalized solid angle for different distances s, and p = 1cm; q = 0.2cm is showing in Figure 5.

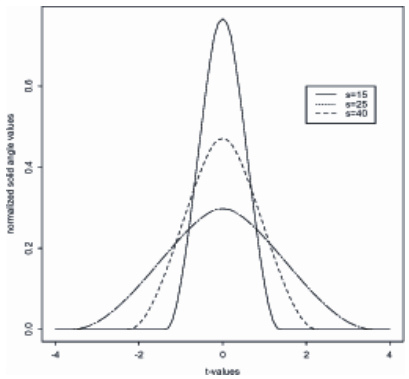

Figure 5. Normalised solid angle for different distances s=15, 25, 40 cm.

5. Approximate solid angle of view

[6] investigate the case where the camera is far away from the body, that is $s >> p, q, t$ then $(s-p)$ and $(s+p) \to s$. On the assumption that the two discs are of equal radius, $d = \left(\frac{2p}{s}\right)t$

and $r_1 = r_2 = q$. The overlap area A is given by $A = q^2 f\left(\frac{pt}{sq}\right)$, where

$f\left(\frac{pt}{sq}\right) = 2\left\{\cos^{-1}\left(\frac{pt}{sq}\right) - \left(\frac{pt}{sq}\right)\sqrt{1-\left(\frac{pt}{sq}\right)^2}\right\}$, and solid angle which is given by:

$\theta(s,t)^{approx} = \tan^{-1}\left[\frac{A}{s^2}\right] = \tan^{-1}\left[\frac{q^2}{s^2} f\left(\frac{pt}{sq}\right)\right]$. For small θ(s,t) and considering the first-order approximation, the approximate solid angle is given $\theta(s,t)^{approx} \approx \left[\frac{q^2}{s^2} f\left(\frac{pt}{sq}\right)\right]$. This formula works successfully when the camera is a long way from the body, but if the distance is small the assumption is not appropriate.

6. Experiments

For the comparison of both formulae three different multihole camera types [8, 9] are considered with collimator tube measurements given in Table 1.

Camera	1	2	3
Half-length (p) cm	2.5	5.0	1.0
Diameter (q) cm	0.5	0.3	0.2

Table 1: Collimator tube dimensions for various gamma cameras.

Extensive comparison of the two forms shows that when the camera is far away from the body the solid angles are almost identical. When the camera is close to the body the differences between the two forms are very small. So there is reason to question whether these differences are significant. If they are, then what critical distance (s_{crit}) could be used to classify when the camera is close to, or far away from the body. A measure used to investigate the differences between exact and approximate solid angle formulae is given in the following proposition [7]:

Proposition 1: The error $E_u(s)$, which calculates the difference between the approximate and exact solid angle is given by the formula:

$$E_u(s) = \left(\sum \left|\theta^{approx}(s,t) - \theta^{exact}(s,t)\right|^u\right)^{1/u}$$

then the critical distance (s_{crit}) is the solution of $E_u(s) = \theta_{crit}$, where θ_{crit} is the critical angle, which is considered to be an important difference. When u=1 then $E_1(s)$ is the absolute error (city-bock distance); when u=2, then $E_2(s)$ is the root squared error (Euclidean distance). The error function corresponding to different distances is illustrated in Figure 6.

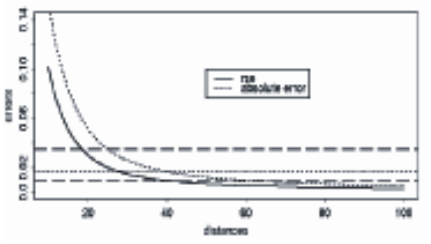

Camera 1

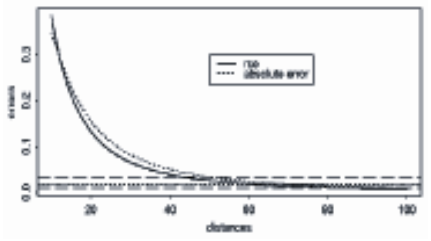

Camera 2

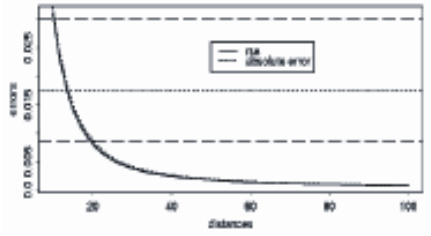

Camera 3

Figure 6. Errors function for the various gamma cameras. The horizontal lines represent the θ_{crit} values: 2^o, 1^o and 0.5^o. The intersection of the error functions and θ_{crit} lines gives an indication of the smallest acceptable distance beyond which the approximate solid angle formula should not be used.

From this graph it can be seen that as the distance increases the error function decreases and eventually the differences are very small ($E_u \to 0$ as $s \to \infty$). The horizontal lines represent critical angles which are compared with the error values. The critical angle specifies how close to zero the error must be. As θ_{crit} gets smaller, the critical distance s_{crit} gets bigger. Four θ_{crit} are considered, which are given in table 2. This table gives the critical distances using different critical angles for various camera parameters.

Critical distances (cm)						
Degree (Radians)	Camera 1		Camera 2		Camera 3	
	E_1	E_2	E_1	E_2	E_1	E_2
2^o (0.0349)	25	18	49	42	11	10
1^o (0.0174)	39	27	71	62	14	13
$(0.5)^o$ (0.0087)	67	43	99	87	20	19
$(0.25)^o$ (0.0043)	*	76	*	*	28	27

Table 2: Critical distances for various critical angles. Below these distances the approximate solid angle formula should not be used. (* Indicates that the critical distance is greater than 100cm.)

For example using $\theta_{crit} = 0.5^o$ and using E_2 as measure of comparison, the critical distance for camera 1 is 43cm for camera 2 is 87cm and for camera 3 is 19cm; after this distance the approximate formula for the solid angle is applicable, and the differences between the two formulae are negligible.
Comparisons of the reconstructions applying [10] work, using exact and approximate solid angle formulae (for p = 1cm; q = 0.2cm) are considered for various distances (s=15, 25cm). Measure for comparison has be considered the Root Square Error (RSE) between reconstruct and truth, number of iterations for the convergences of the algorithm and CPU execution time. For the artificial truth representation, two circles are considered which represent a solid inner cylinder placed centrally within a larger hollow cylinder. The radius of the inner circle is $r_2 = 8$cm and the radius of the outside circle is $r_1 = 12$cm (Figure 7a).

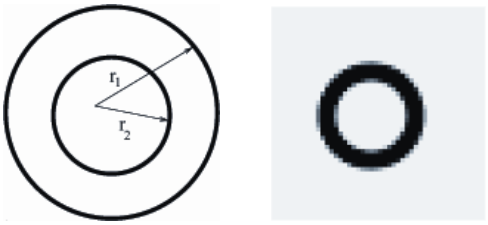

(a) (b)

Figure 7. (a) Description of artificial truth; (b) 2-dimensional representation

This “truth" is similar to the phantom used by [11] and represents a simplified 3d model of the left ventricular myocardium with homogeneous uptake of Tl -201 (Figure 7b). Reconstructions for different distances using both formulae are illustrated in Figure 8.

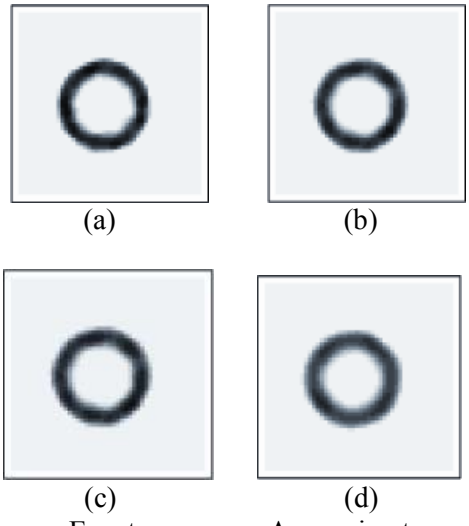

(a) (b)

(c) (d)

Exact Approximate

Figure 8. Comparison between exact (a, c) and approximate (b, d) solid angle of view for distance s=15cm (a, b) and s=25cm (c, d).

As it is expected when the camera is close to the body (s=15 cm) the reconstruction is better. Homogeneous regions appear with sharper boundaries. The algorithm converges to the final reconstruction after 723 iterations for exact with RSE equals to 240.22 and 793 iterations for approximate form with RSE equals to 248.75. The running time is increasing with 3.45min for exact to 4.12min for approximate. When the distance is large (s=25 cm) the homogeneous regions are still apparent but with smoother boundaries. The number of iterations is increased with values 814 iterations for exact and 826 iterations for approximate form. The extra smoothing at the boundaries has the effect of increasing the RSE, with values 263.72 for exact and 270.64 for approximate form. The running time is increasing with 6.50min for exact to 7.20min for approximate. As the distance increases the number of iterations, the running time and the RSE increase. The higher values of RSE indicate that the degree of smoothness is larger when the camera is far away. The algorithm is quicker to converge for small distances and hence the running time is shorter. The algorithm was rerun for different starting images to compare performance; it appeared that this has no effect.

7. Conclusions

An important part of the weights calculation considers the geometry of the gamma camera system and defines the angle of view.

Experimental results show that the shape of the angle of view formula leads to unsatisfactory reconstructions. The solution of this problem is the consideration of: (i) the relationship between the number of detectors and the number of body pixels, and (ii) the solid angle of view. In the first case the number of detectors must be at least equal to the number of pixels. The second concerns the derivation of the solid angle of view.

The usual assumption, in deriving the solid angle of view, is that the camera is a long way from the body; this case was studied by [6]. When this assumption is incorrect, the resulting reconstructions may not be sufficiently accurate. An exact formula for solid angle was derived which is valid for all distances. For the comparison between exact and approximate solid angle, various camera parameters was used and critical distances are introduced.

Visual and quantitative comparison of the reconstructions showed that the exact solid angle performs better compared to the approximate solid angle. When the camera is close to the body (small distances) the reconstructions are close to the truth with sharp boundaries, the algorithm needs few iterations to converge, and the RSE measure is small. When the camera is far away (large distances) the reconstructions become smoother, the algorithm needs more iterations and the RSE measure is larger.

Reference:

[1] Jaszczak R.J, Coleman R.E, Whitehead FR (1981): Physical factors affecting quantitative measurements using camera-based single photon emission tomography (SPECT), *IEEE Trans. Nucl. Sci.,* 28:69-80.

[2] S. Geman, K.M. Manbeck and D. E. McClure (1991): A comprehensive statistical model for single photon emission tomography, *Report in Pattern Analysis, Brown University, 153.*

[3] F. H. Attix (1983): *Introduction to radiological physics and Radiation dosimetry*, John Wiley & Sons, New York.

[4] J. A. Sorenson and M. E. Phelps (1987): *Physics in Nuclear Medicine*, Second edition, Grune & Stratton, Orlando.

[5] S. A. Larsson (1980): Gamma camera emission tomography, *Acta Radiologica, Supplementum* 363, Stockholm.

[6] I. S. Weir and P. J. Green (1994): Modeling data from single photon emission computed tomography, *Advances in Applied Statistics,* 313-338.

[7] S. Zimeras (1997): Statistical models in medical image processing, Ph. D. Thesis, University of Leeds, UK.

[8] N. F. Moody, W. Paul and M. L. G. Joy (1970): A survey of medical gamma-ray cameras, *Proceedings of the IEEE,* vol. 58(2), 217-242.

[9] G. V. Guru, J. D. Valentine, D. K. Wehe and G. F. Knoll (1994): Monte carlo modeling of a multiple-hole collimator for high energy gamma-ray imaging, *IEEE Trans. of Nuclear Science*, vol. 41, 898-902.

[10] P. J. Green (1990): Bayesian reconstructions from emission tomography data using a modified EM algorithm, *IEEE Trans Medical Imaging*, 9, 84-93.

[11] P. J. Maniawski, H. T. Morgan, and F. J. Walkers (1991). Orbit-related variation in spatial resolution as a source of artificial defect in Thallium-201 SPECT, *J. Nuclear Medicine*, 32, 871-875.